EPJ manuscript No.
(will be inserted by the editor)

High-accuracy neutron diffusion calculations based on integral transport theory

Roy Gross[1], Daniele Tomatis[2], and Erez Gilad[1a]

[1] The Unit of Nuclear Engineering, Ben-Gurion University of the Negev, 8410501 Beer-Sheva, Israel
[2] CEA, DEN, Service d'études des réacteurs et de mathématiques appliquées (SERMA), Université Paris-Saclay, F-91191 Gif-sur-Yvette, France

Received: date / Revised version: date

Abstract In this paper, the Ronen method is developed, implemented and applied to resolve the neutron flux and the criticality eigenvalue in a simple homogeneous problem. The Ronen method is based on iterative calculations of the multigroup diffusion coefficients using a multigroup diffusion model and driven by the solutions of the integral transport equation. The local diffusion constants are modified in order to reproduce new estimates of the surface currents by a transport operator. The diffusion solver employed in this study uses finite differences and the transport-corrected currents are introduced into the numerical scheme by means of drift terms. The corrected solutions are compared against reference results obtained by a discrete ordinate code. Boundary conditions are discussed and proper approximations are introduced in order to conserve the particle balance. The results match extremely well the reference solutions, especially in the limit of fine meshes, but slow convergence of the scalar flux is reported.

Key words. neutron diffusion – integral transport – non-linear transport correction

PACS. 28.00.00 Nuclear engineering and nuclear power studies – 28.20.Gd Neutron transport: diffusion and moderation – 05.60.-k Transport processes – 28.41.-i Fission reactors

1 Introduction

Neutron transport calculations on a full core scale can be a highly intensive computational task. High-fidelity core design optimization or transient analyses can quickly become computationally impractical when using transport methods [1]. For example, in order to achieve a 1% accuracy in the local flux/power estimation, an order of 10^{11} histories is needed in a full-core Monte Carlo calculation [2]. Another problem is the huge number of variables and parameters to be stored and used during computation, e.g., tallies, geometry, cross sections, and depletion data. A conservative estimation of the memory needed for reasonably accurate full-core Monte Carlo neutronic calculation is in the range of terabytes (TBs) [2].

To overcome this difficulty, faster (and less accurate) multigroup neutron diffusion solvers are frequently used [3,4]. However, future Gen-IV reactor designs are characterized by strong heterogeneity in the core, e.g., axial and radial seed-blanket structures, as in the French ASTRID SFR CVF design [5], challenging the accuracy of diffusion calculations. Moreover, modern calculation schemes evolve towards so-called "best-estimate" codes, aiming at high accuracy [6].

A crucial issue in obtaining an accurate diffusion calculation is the formulation of the diffusion coefficient [7, 8]. The calculation of this parameter should be based on physical insights from the transport equation such that the resulting improved ("transport corrected") diffusion approximation can capture the transport phenomena of interest. Such transport corrections can be divided into two main classes. The first class is based on extending the P_1 model equations (and the associated boundary conditions) along with some closure scheme, such as the well-known SP_3 approximation [9]. The second class, to which this study belongs, is based on the re-calculation of the diffusion coefficients within the multigroup diffusion framework [10].

In this paper, the development, implementation, and qualification of the Ronen Method [11] in one-dimensional homogeneous plane geometry is reported. This method is implemented as a highly accurate multigroup neutron diffusion solver based on novel transport corrections. The main hypothesis underlying the Ronen method is based

[a] e-mail: gilade@bgu.ac.il (corresponding author)

on iterative calculations of the multigroup diffusion coefficients driven by the solutions of the integral transport equation [10, 11].

The theoretical background is detailed in Section 2, the numerical implementation is described in Section 3, the results are presented in Section 4 and conclusions are brought in Section 5.

2 Theoretical background

2.1 The Ronen method

In 2004, Ronen [11] suggested to derive corrected diffusion coefficients using Fick's law and more accurate estimations of the neutron currents by means of integral transport operators, whereas the neutron flux is resolved by diffusion theory. Denoting the integral transport and diffusion currents by $\boldsymbol{J}_{\rm tr}(\boldsymbol{r}, E)$ and $\boldsymbol{J}_D(\boldsymbol{r}, E)$, respectively, the Ronen idea is based on changing the diffusion coefficient such that

$$\boldsymbol{J}_D(\boldsymbol{r}, E) = -D(\boldsymbol{r}, E)\boldsymbol{\nabla}\phi(\boldsymbol{r}, E) = \boldsymbol{J}_{\rm tr}(\boldsymbol{r}, E) \ . \tag{1}$$

Since these accurate estimates of the currents are based on a known flux distribution, it was also suggested to execute new diffusion calculations, thus updating iteratively the diffusion coefficients in the global calculation.

$$D^{(k+1)}(\boldsymbol{r}, E) = -\boldsymbol{J}^{(k)}_{\rm tr}(\boldsymbol{r}, E)\left[\boldsymbol{\nabla}\phi^{(k)}(\boldsymbol{r}, E)\right]^{-1} \ , \tag{2}$$

where k is the iteration index. The use of a tensor notation is needed for the diffusion coefficient in general multidimensional problems.

The motivation for this method was to overcome the inherent limitation of Fick's law requiring smooth flux gradients and thus small neutron absorption rate with respect to scattering in general. Nevertheless, isotropic scattering remained as a basic postulate. For example, in a one-dimensional homogeneous slab with void boundary conditions, Eq. (2) takes the following form [11]

$$D^{(k+1)}(x, E) = -\frac{\frac{1}{2}\int_0^a dx' E_2[\sigma(E)|x - x'|]\text{sign}(x - x')q^{(k)}(x', E)}{\partial\phi^{(k)}(x, E)/\partial x} \ . \tag{3}$$

This idea was later used by Tomatis and Dall'Osso [10], who provided a numerical demonstration in a simple slab problem. Instead of updating the diffusion coefficient by the ratio of the current and the flux gradient, as in Fick's law, they adopted the Coarse Mesh Finite Differences method (CMFD) for taking into account the new currents estimated by the integral transport operator in the diffusion solver. This technique, largely adopted in the literature of nodal methods [3, 12], can avoid indeterminate divisions in case of vanishing flux gradients. They tested this implementation in a homogeneous bare slab using two-group cross sections representative of a realistic PWR assembly. It was observed that the Ronen method (RM) could drive the flux distribution away from diffusion and closer to the reference solution of the integral Boltzmann transport equation, regardless of the initial formulation used for the diffusion coefficient. As expected, the largest errors were located near the boundary, where the transport effects are most pronounced, slowly decreasing even after many iterations.

2.2 The one-dimensional Peierls equation

There are several ways to drive the integral expression for the flux in slab geometry. Most of them start with assuming homogeneous and isotropic scattering and sources, yielding the *Peierls equation* [7,13–17]. The derivation of expression for slab geometry (of thickness a) is straightforward, yielding

$$\begin{aligned}\phi(x, E) &= \frac{1}{2}\int_0^a dx' E_1\left[\sigma(E)|x - x'|\right] q(x', E) \\ &= \frac{1}{2}\int_0^a dx' E_1\left[\sigma(E)|x - x'|\right]\left[\int_0^\infty dE'\sigma_s(E \leftarrow E')\phi(x', E') + S(x', E)\right] \ ,\end{aligned} \tag{4}$$

where $E_1(x)$ is a first order exponential integral [18]. Note that this expression does not include the contribution of uncollided neutrons originate from the flux at the boundaries.

Another starting point for the derivation of the integral expression for the flux in slab geometry is to directly integrate along a line the transport equation [13, 15–17]

$$\psi(\boldsymbol{r},\hat{\boldsymbol{\Omega}}) = \int_0^R dR' q(\boldsymbol{r}-R'\hat{\boldsymbol{\Omega}},\hat{\boldsymbol{\Omega}}) e^{-\tau(\boldsymbol{r},\boldsymbol{r}-R'\hat{\boldsymbol{\Omega}})} + \psi(\boldsymbol{r}-R\hat{\boldsymbol{\Omega}},\hat{\boldsymbol{\Omega}}) e^{-\tau(\boldsymbol{r},\boldsymbol{r}-R\hat{\boldsymbol{\Omega}})} \ , \tag{5}$$

where $\tau(\boldsymbol{r},\boldsymbol{r}-R'\hat{\boldsymbol{\Omega}})$ is the *optical length*, defined as

$$\tau(\boldsymbol{r},\boldsymbol{r}-R'\hat{\boldsymbol{\Omega}}) \equiv \int_0^{R'} \sigma(\boldsymbol{r}-R''\hat{\boldsymbol{\Omega}}) dR' \ . \tag{6}$$

Assuming isotropic scattering and homogeneous medium in one-dimension for Eq. (5) recovers Eq. (4).

In what follows, a generalization of Eq. (4) is derived for heterogeneous medium with anisotropic scattering.

2.3 Integral expressions for the neutron flux & current

Consider an infinite one-dimensional slab of width a. The angular flux in the slab is given by [17]

$$\psi(x,E,\mu) = \psi(0,E,\mu)e^{-\tau(0,x,E)/\mu} + \int_0^x dx' \ \frac{Q(x',E,\mu)}{\mu} e^{-\tau(x',x,E)/\mu} \ , \qquad \mu>0 \ , \tag{7a}$$

$$\psi(x,E,\mu) = \psi(a,E,\mu)e^{\tau(x,a,E)/\mu} - \int_x^a dx' \ \frac{Q(x',E,\mu)}{\mu} e^{\tau(x,x',E)/\mu} \ , \qquad \mu<0 \ , \tag{7b}$$

where

$$\tau(x',x,E) \equiv \int_{x'}^x \sigma(x'',E) dx'' \tag{8}$$

and $Q(x,E,\mu)$ denotes all sources.

The angular dependence of the source and the uncollided boundary flux terms is expanded in a series of orthogonal Legendre polynomials

$$\begin{aligned} \psi(0,E,\mu) &= \sum_{l=0}^{\infty} \frac{2l+1}{2} \psi_l(0,E) P_l(\mu) \\ \psi(a,E,\mu) &= \sum_{l=0}^{\infty} \frac{2l+1}{2} \psi_l(a,E) P_l(\mu) \ . \end{aligned} \tag{9}$$

The source cross sections are written explicitly as [10]

$$\sigma_l(x,E\leftarrow E')dE' = \sigma_{s,l}(x,E\leftarrow E')dE' + \delta_{l0}\frac{\chi(E)}{k_{\text{eff}}}\nu\sigma_f(x,E')dE' \tag{10}$$

and the source term is expanded

$$\begin{aligned} Q(x,E,\mu) &= \sum_{l=0}^{\infty} \frac{2l+1}{2} \int_0^{\infty} dE' \sigma_{s,l}(x,E\leftarrow E')\psi_l(x,E')P_l(\mu) + \frac{\chi(E)}{2k_{\text{eff}}} \int_0^{\infty} dE' \nu\sigma_f(x,E')\psi_0(x,E') \\ &= \sum_{l=0}^{\infty} \frac{2l+1}{2} \int_0^{\infty} dE' \sigma_l(x,E\leftarrow E')\psi_l(x,E')P_l(\mu) \\ &= \sum_{l=0}^{\infty} \frac{2l+1}{2} \int_0^{\infty} dE' q_l(x,E\leftarrow E')P_l(\mu) \\ &= \sum_{l=0}^{\infty} \frac{2l+1}{2} q_l(x,E)P_l(\mu) \ , \end{aligned} \tag{11}$$

where the source angular moments are defined as

$$q_l(x,E) \equiv \int_0^{\infty} dE' q_l(x,E\leftarrow E') \equiv \int_0^{\infty} dE' \sigma_l(x,E\leftarrow E')\psi_l(x,E')dE' \ . \tag{12}$$

In order to calculate the scalar flux ϕ^+ at x resulting from neutrons coming from the left, i.e., $x' < x$ ($\mu > 0$), substitute Eqs. (9) in Eq. (7a) and integrate over the angle

$$\begin{aligned}\phi^+(x,E) &\equiv \int_0^1 d\mu\psi(x,E,\mu) \\ &= \sum_{l=0}^{\infty}\frac{2l+1}{2}\left\{\psi_l(0,E)\int_0^1 d\mu P_l(\mu)e^{-\tau(0,x,E)/\mu} + \int_0^x dx' q_l(x',E)\int_0^1 d\mu\frac{P_l(\mu)}{\mu}e^{-\tau(x',x,E)/\mu}\right\} . \end{aligned} \tag{13}$$

In order to solve the angular integrals we resort to the following result [19, 20]

$$\int_0^1 \mu^i P_l(\mu)e^{-y/\mu}d\mu = \sum_{m=0}^{[l/2]} h_m E_{l+2+i-2m}(y) , \tag{14}$$

where h_m is defined according to

$$P_l(x) = \sum_{m=0}^{[l/2]} h_m x^{n-2m} \tag{15}$$

and given explicitly by

$$h_m = \frac{(-1)^m(2l-2m)!}{2^l m!(l-m)!(l-2m)!} \tag{16}$$

where

$$[l/2] = \begin{cases} l/2, & l \text{ even}, \\ (l-1)/2, & l \text{ odd}. \end{cases} \tag{17}$$

Hence, the contribution to the flux from $x' < x$ can be written as

$$\phi^+(x) = \sum_{l=0}^{\infty}\frac{2l+1}{2}\sum_{m=0}^{[l/2]} h_m\left\{E_{l+2-2m}[\tau(0,x,E)]\psi_l(0,E) + \int_0^x dx' E_{l+1-2m}[\tau(x',x,E)]q_l(x',E)\right\} . \tag{18}$$

The contribution to the flux from $x' > x$ ($\mu < 0$) can be calculated in a similar manner, using the change of variables $\eta = -\mu$ for the angular integrals and the fact that $P_l(-\mu) = (-1)^l P_l(\mu)$, resulting in an expression for the scalar flux which accounts for anisotropic scattering and heterogeneous medium

$$\begin{aligned}\phi(x,E) &= \phi^+(x,E) + \phi^-(x,E) \\ &= \sum_{l=0}^{\infty}\frac{2l+1}{2}\sum_{m=0}^{[l/2]} h_m\Big\{E_{l+2-2m}[\tau(0,x,E)]\psi_l(0,E) + (-1)^l E_{l+2-2m}[\tau(x,a,E)]\psi_l(a,E) \\ &\quad + \int_0^x dx' E_{l+1-2m}[\tau(x',x,E)]q_l(x',E) + (-1)^l\int_x^a dx' E_{l+1-2m}[\tau(x,x',E)]q_l(x',E)\Big\} . \end{aligned} \tag{19}$$

The generalization of Eq. (19) to current is obtained in a similar procedure according to

$$\begin{aligned}J(x,E) &= J^+(x,E) - J^-(x,E) = \int_0^1 d\mu\mu\psi(x,E,\mu) - \int_0^{-1} d\mu\mu\psi(x,E,\mu) \\ &= \sum_{l=0}^{\infty}\frac{2l+1}{2}\sum_{m=0}^{[l/2]} h_m\Big\{E_{l+3-2m}[\tau(0,x,E)]\psi_l(0,E) + (-1)^{l+1}E_{l+3-2m}[\tau(x,a,E)]\psi_l(a,E) \\ &\quad + \int_0^x dx' E_{l+2-2m}[\tau(x',x,E)]q_l(x',E) + (-1)^{l+1}\int_x^a dx' E_{l+2-2m}[\tau(x,x',E)]q_l(x',E)\Big\} . \end{aligned} \tag{20}$$

3 Numerical implementation

The cross sections, as well as the diffusion coefficient, are usually available as volume-averaged data per cell in the mesh. Once the scalar flux is known from the finite differences solver using the original diffusion coefficients, the integral expressions derived in Section 2.3 can be used to get new estimates of the currents J at the cell interfaces.

Instead of computing new diffusion coefficients on the interfaces by Fick's law, $J_D(x,E) = -D(E)\partial_x\phi(x,E)$, new corrective currents $\delta J(x_s,E) = J_{\rm tr}(x_s,E) - J_D(x_s,E)$ are obtained on cell interfaces x_s. Here, $J_D(x,E)$ is called the "diffusion current" and is obtained using Fick's law, with the original values of the homogeneous diffusion coefficients and with the derivative approximated by finite differences. In one-dimensional geometry and using the notation in Fig. 1, the diffusion current and the corrective current are evaluated according to

$$\begin{aligned} J_D(x_{i+1/2},E) &\cong -D(x_{i+1/2},E)\frac{\phi(x_{i+1},E)-\phi(x_i,E)}{(\Delta x_{i+1}+\Delta x_i)/2} \\ \delta J(x_{i+1/2},E) &= -\delta D(x_{i+1/2},E)\frac{\phi(x_{i+1},E)+\phi(x_i,E)}{(\Delta x_{i+1}+\Delta x_i)/2} \ , \end{aligned} \tag{21}$$

where integer and rational subscripts indicate node-averaged and interface quantities, respectively. The discretized form of the current δJ must involve the neighboring flux as well, but its representation is changed into a drift-advection term to get rid of possible undefined division by zeros in case of flat flux [10, 12]. The so-called "transport current" $J_{\rm tr}(x_s,E)$ is evaluated using the integral expression derived in Section 2.3 as described in Section 3.2.

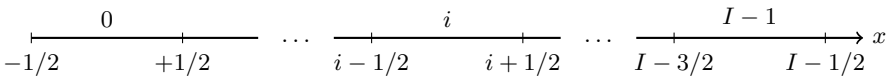

Figure 1. Notation of the one-dimensional mesh.

Since the input diffusion coefficients are provided as node averaged, and they are always needed at interfaces, they are approximated by local volume averages:

$$D(x_{i+1/2},E) = \frac{\Delta x_i D(x_i,E) + \Delta x_{i+1} D(x_{i+1},E)}{\Delta x_i + \Delta x_{i+1}} \ . \tag{22}$$

3.1 The correction as a drift term

The new numerical corrections δD are obtained on the interfaces using Eq. (21) to be used in the finite differences solver, together with the diffusive currents from Eq. (21). Hence, the neutron balance resolved by the CMFD takes into account both types of currents J_D and δJ. Hence, the one-dimensional multigroup neutron balance CMFD diffusion equations actually solved are

$$J^+_{D,g}(x) + \delta J^+_{D,g}(x) - J^-_{D,g}(x) - \delta J^-_{D,g}(x) + \sigma_g\phi_g(x) = \frac{\chi_g}{k_{\rm eff}}\sum_{g'=1}^{G}\nu\sigma_{f,g'}(x)\phi_{g'}(x) + \sum_{g'=1}^{G}\sigma_{s,g\leftarrow g'}\phi_{g'}(x) \ , \tag{23}$$

where $J^\pm_{D,g}(x) \equiv J_{D,g}(x_{i\pm1/2})$.

Using the definitions in Eqs. (21) and (22) and Fig. 1, the discretized form of Eq. (23) is

$$\begin{aligned} -2D^g_{i+1/2}\frac{\phi_{i+1,g}-\phi_{i,g}}{\Delta x_{i+1}+\Delta x_i} - 2\delta D^g_{i+1/2}\frac{\phi_{i+1,g}+\phi_{i,g}}{(\Delta x_{i+1}+\Delta x_i)} + 2D^g_{i-1/2}\frac{\phi_{i,g}-\phi_{i-1,g}}{\Delta x_i+\Delta x_{i-1}} + 2\delta D^g_{i-1/2}\frac{\phi_{i,g}+\phi_{i-1,g}}{(\Delta x_i+\Delta x_{i-1})} \\ + \sigma^g_i\phi_{i,g} = \sum_{g'=1}^{G}\sigma^{g\leftarrow g'}_{s,i}\phi_{i,g'} + \frac{\chi_g}{k_{\rm eff}}\sum_{g'=1}^{G}\nu\sigma^{g'}_{f,i}\phi_{i,g'} \ . \end{aligned} \tag{24}$$

Rearranging terms to get

$$\begin{aligned} \left(\frac{-D^g_{i-1/2}+\delta D^g_{i-1/2}}{\Delta x_{i-1}+\Delta x_i}\right)\phi_{i-1,g} + \left[\frac{D^g_{i+1/2}-\delta D^g_{i+1/2}}{\Delta x_{i+1}+\Delta x_i} + \frac{D^g_{i-1/2}+\delta D^g_{i-1/2}}{\Delta x_i+\Delta x_{i-1}} + \frac{\sigma^g_i}{2}\right]\phi_{i,g} \\ + \left(\frac{-D^g_{i+1/2}-\delta D^g_{i+1/2}}{\Delta x_{i+1}+\Delta x_i}\right)\phi_{i+1,g} = \frac{1}{2}q_{i,g} \ , \end{aligned} \tag{25}$$

where $q_{i,g}$ is the RHS of Eq. (24).

These equations can be formulated in operators notation according to

$$\mathcal{M}\Phi = \frac{1}{k_{\text{eff}}}\mathcal{F}\Phi \ , \tag{26}$$

where $\mathcal{M}$ is the migration operator, whose entries are given by Eq. (25) making it a three-diagonal banded matrix, and $\mathcal{F}$ is the neutron generation operator given by $q_{i,g}$. Note that $\mathcal{M}$ can be written as $\mathcal{M} = \mathcal{M}_0 + \delta\mathcal{M}$ distinguishing the diffusion corrections from the constant diffusion coefficients derived from the transport problem. In the homogeneous case, $\mathcal{M}(x) = \mathcal{M}_0 + \delta\mathcal{M}(x)$.

3.2 Calculation of the integral currents

The numerical evaluation of the neutron current $J(x, E)$ at cell interfaces requires spatial integration of Eq. (20). The neutron current at any interface can be calculated by considering separately contributions from all cells who are to the left or to the right of the interface. The current at a cell interface is discretized as follows

$$\begin{aligned} J_g(x_{i+1/2}) = \sum_{l=0}^{\infty} \frac{2l+1}{2} \sum_{m=0}^{[l/2]} h_m \Bigg\{ & E_{n_{l,m}+1}[\tau_g(0, x_{i+1/2})]\psi_{l,g}(0) + (-1)^{l+1} E_{n_{l,m}+1}[\tau_g(x_{i+1/2}, a)]\psi_{l,g}(a) \\ & + \sum_{j=0}^{i} q_{l,g,j} \int_{x_{j-1/2}}^{x_{j+1/2}} dx' E_{n_{l,m}}[\tau_g(x', x_{i+1/2})] + (-1)^{l+1} \sum_{j=i+1}^{I-1} q_{l,g,j} \int_{x_{j-1/2}}^{x_{j+1/2}} dx' E_{n_{l,m}}[\tau_g(x_{i+1/2}, x')] \Bigg\} \ , \end{aligned} \tag{27}$$

where $n_{l,m} \equiv l + 2 - 2m$. The source $q_{l,g,j}$ is the l^{th} angular moment of the volume-average within-group source in the cell j. The optical lengths show the subscript g because they are evaluated with the corresponding total cross section σ_g. Note that for void boundary conditions, the boundary terms vanish by definition. The spatial integrals in Eq. (27) can be solved analytically knowing that $E'_{n+1}(u) = -E_n(u)$ [21]. Using the notation in Fig. 2, the optical length between the right surfaces of cell j and cell i is

$$\Xi^g_{i,j} \equiv \begin{cases} \Xi^g_{i \geqslant j} = \sum\limits_{k=j+1}^{i} \sigma_{g,k} \Delta x_k & x \geqslant x' \quad (i \geqslant j) \\ \Xi^g_{i<j} = \sum\limits_{k=i+1}^{j-1} \sigma_{g,k} \Delta x_k & x < x' \quad (i < j) \ . \end{cases} \tag{28}$$

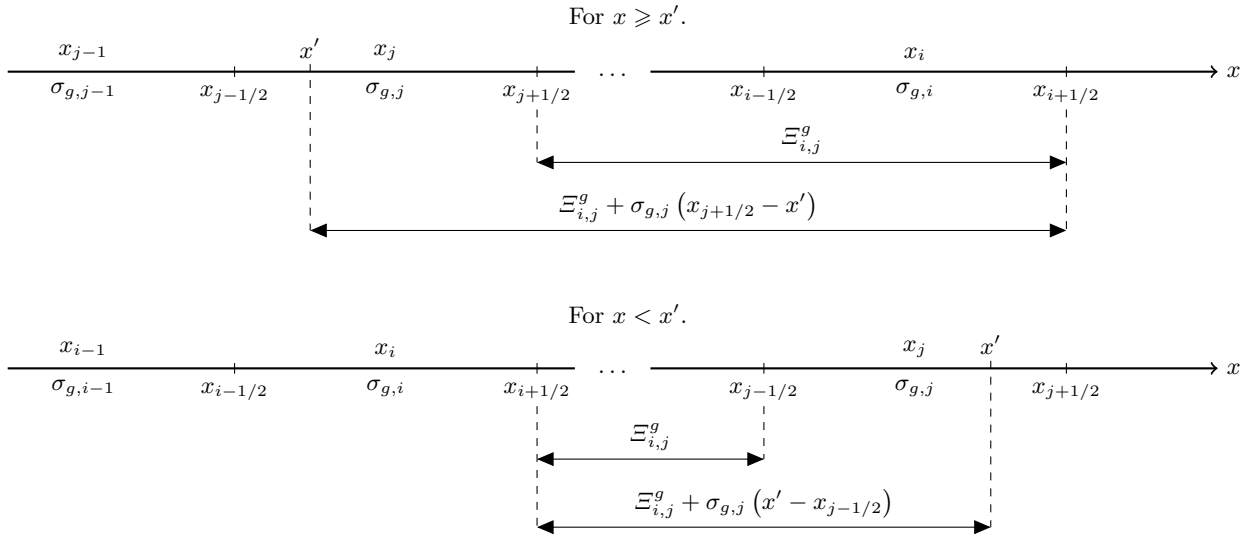

Figure 2. Notation for numerical evaluation of integral interface currents.

Substituting

$$u = \begin{cases} \Xi^g_{i \geqslant j} + \sigma_{g,j}(x_{j+1/2} - x') & x' \leqslant x \quad (j \leqslant i) \\ \Xi^g_{i<j} + \sigma_{g,j}(x' - x_{j-1/2}) & x' > x \quad (j > i) \ , \end{cases} \tag{29}$$

and integrating the $E_{n_{l,m}}$ terms in Eq. (27) yields

$$\begin{aligned}
\int_{x_{j-1/2}}^{x_{j+1/2}} dx' E_{n_{l,m}}[\tau_g(x', x_{i+1/2})] &= \frac{1}{\sigma_{g,j}} \left[E_{n_{l,m}+1}(\Xi^g_{i \geqslant j}) - E_{n_{l,m}+1}(\Xi^g_{i \geqslant j} + \sigma_{g,j} \Delta x_j) \right] \\
&= \frac{1}{\sigma_{g,j}} \left\{ E_{n_{l,m}+1} \left[\tau_g(x_{j+1/2}, x_{i+1/2}) \right] - E_{n_{l,m}+1} \left[\tau_g(x_{j-1/2}, x_{i+1/2}) \right] \right\} \\
\int_{x_{j-1/2}}^{x_{j+1/2}} dx' E_{n_{l,m}}[\tau_g(x_{i+1/2}, x')] &= \frac{1}{\sigma_{g,j}} \left[E_{n_{l,m}+1}(\Xi^g_{i<j}) - E_{n_{l,m}+1}(\Xi^g_{i<j} + \sigma_{g,j} \Delta x_j) \right] \\
&= \frac{1}{\sigma_{g,j}} \left\{ E_{n_{l,m}+1} \left[\tau_g(x_{i+1/2}, x_{j-1/2}) \right] - E_{n_{l,m}+1} \left[\tau_g(x_{i+1/2}, x_{j+1/2}) \right] \right\} \ . \qquad (30)
\end{aligned}$$

Hence, the interface currents can be written as

$$\begin{aligned}
J_g(x_{i+1/2}) = \sum_{l=0}^{\infty} \frac{2l+1}{2} \sum_{m=0}^{[l/2]} h_m \Bigg\{ & E_{n_{l,m}+1}[\tau_g(0, x_{i+1/2})] \psi_{l,g}(0) + (-1)^{l+1} E_{n_{l,m}+1}[\tau_g(x_{i+1/2}, a)] \psi_{l,g}(a) \\
& + \sum_{j=0}^{i} \frac{q_{l,g,j}}{\sigma_{g,j}} \left\{ E_{n_{l,m}+1} \left[\tau_g(x_{j+1/2}, x_{i+1/2}) \right] - E_{n_{l,m}+1} \left[\tau_g(x_{j-1/2}, x_{i+1/2}) \right] \right\} \\
& + (-1)^{l+1} \sum_{j=i+1}^{I-1} \frac{q_{l,g,j}}{\sigma_{g,j}} \left\{ E_{n_{l,m}+1} \left[\tau_g(x_{i+1/2}, x_{j-1/2}) \right] - E_{n_{l,m}+1} \left[\tau_g(x_{i+1/2}, x_{j+1/2}) \right] \right\} \Bigg\} \ . \qquad (31)
\end{aligned}$$

Note that for the isotropic case ($l = 0$) Eq. (31) reduces to

$$\begin{aligned}
J_g(x_{i+1/2}) &= \frac{1}{2} \Bigg\{ E_3[\tau_g(0, x_{i+1/2})] \psi_{0,g}(0) - E_3[\tau_g(x_{i+1/2}, a)] \psi_{0,g}(a) \\
&\quad + \sum_{j=0}^{i} \frac{q_{0,g,j}}{\sigma_{g,j}} \left\{ E_3 \left[\tau_g(x_{j+1/2}, x_{i+1/2}) \right] - E_3 \left[\tau_g(x_{j-1/2}, x_{i+1/2}) \right] \right\} \\
&\quad - \sum_{j=i+1}^{I-1} \frac{q_{0,g,j}}{\sigma_{g,j}} \left\{ E_3 \left[\tau_g(x_{i+1/2}, x_{j-1/2}) \right] - E_3 \left[\tau_g(x_{i+1/2}, x_{j+1/2}) \right] \right\} \Bigg\} \\
&= \frac{1}{2} \Bigg\{ E_3[\tau_g(0, x_{i+1/2})] \psi_{0,g}(0) - E_3[\tau_g(x_{i+1/2}, a)] \psi_{0,g}(a) \\
&\quad + \sum_{j=0}^{I-1} \frac{q_{0,g,j}}{\sigma_{g,j}} \left\{ E_3 \left[\tau_g(x_{j+1/2}, x_{i+1/2}) \right] - E_3 \left[\tau_g(x_{j-1/2}, x_{i+1/2}) \right] \right\} \operatorname{sign}(i-j) \Bigg\} \ . \qquad (32)
\end{aligned}$$

These transfer probabilities $E_{n_{l,m}}[\tau_g(x_i, x_j)]$ are pre-calculated once and are stored in a multi-dimensional array.

3.3 Boundary conditions

A generalized form for the boundary condition (at the left) follows as

$$J_D(x = 0) = \frac{\phi_{i=0}}{\Delta x_0/2 + \zeta} \ , \qquad (33)$$

where ζ is the extrapolation length in case of vacuum. Reflection can be reproduced by $\zeta \to \infty$, whereas the condition of zero-flux is realized by $\zeta = 0$. The quantity δJ at the boundary takes the simpler form of $\delta J = -\delta D_{-1/2} \phi_0$, without dividing by the spatial width, since no particular extrapolation length is appropriate for the correction. The expression for the right boundary is straightforward, implying a non-negative current.

3.4 The Ronen iterative scheme

The Ronen algorithm is described as follows (see Fig. 3):

1. Initialize - the algorithm receives the geometry and the cross sections of the problem as input. At this stage, the corrections to the diffusion coefficients $\delta D^{(0)}(x,E)$ are set to zero and the initial pure-diffusion operator $\mathcal{A}_0(E)$ is constructed. Initial guesses for the flux $\phi^{(0)}(x,E)$ and multiplication factor $k_{\texttt{eff}}^{(0)}$ are set.
2. Diffusion Solver - a one-dimensional multigroup diffusion solver is executed until convergence using the diffusion corrections from the previous iteration $\delta D^{(k)}(x,E)$ through the diffusion operator $\mathcal{A}^{(k)}(x,E) = \mathcal{A}_0(E) + \delta A^{(k)}(x,E)$. The results are an updated estimation of the diffusion flux $\phi^{(k)}(x,E)$ and the multiplication factor $k_{\texttt{eff}}^{(k)}$.
3. Calculate Currents - using the updated diffusion flux $\phi^{(k)}(x,E)$, both the diffusion current $J_D^{(k)}(x,E)$ (Eq. 21) and the transport current $J_{\texttt{tr}}^{(k)}(x,E)$ (Eq. 20) are calculated.
4. Calculate corrections - the diffusion correction $\delta D^{(k+1)}(x,E)$ (Eq. 21) is obtained using $\delta J^{(k)}(x,E)$ and Eq. (21).
5. Update diffusion coefficients - reconstruct the diffusion operator $\mathcal{A}^{(k+1)} = \mathcal{A}_0 + \delta\mathcal{A}^{(k+1)}$ (Eq. 25).
6. If flux and eigenvalue are not converged, go to step 2.

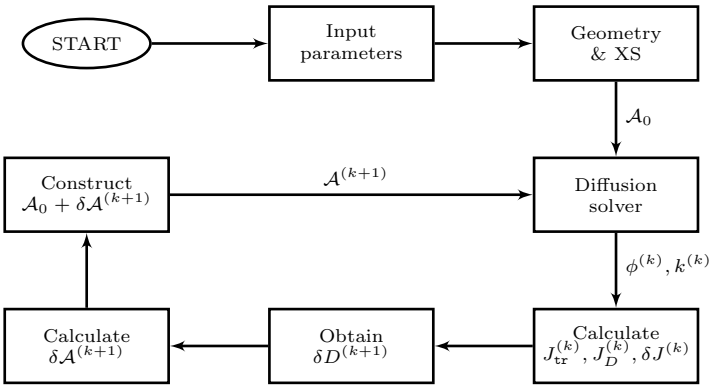

Figure 3. A flow chart of the Ronen algorithm.

4 Results

The reference solution for the one-dimensional homogeneous slab is generated using a Python3 discrete ordinates (S_n) code with $N = 16$ [17]. The diffusion solutions and the Ronen iterations are produced using original codes developed in Pyhton3. All simulations utilize regular mesh in a slab of width $a = 21.5$ cm. All thresholds are set to 1E-6 and no (over/under)-relaxation is done. The initial diffusion coefficient is set to $D = (3\sigma_{tr})^{-1} = (3\sigma)^{-1}$. Void boundary conditions are used (extrapolated distance) at the edges of the slab and they are constant for each energy group. The two-group dataset used in this study is taken from [10] and is shown in Table 1.

Table 1. Two-group dataset used in this study [10].

Group g	σ_g	$\sigma_{s,0,g\leftarrow g'}$		χ_g	$\nu\sigma_{f,g}$
1	5.3115×10^{-1}	5.04664×10^{-1}	2.03884×10^{-3}	1	7.15848×10^{-3}
2	$1.30058\times10^{+0}$	1.62955×10^{-2}	$1.19134\times10^{+0}$	0	1.41284×10^{-1}

Table 2 shows the reactivity differences as a function of mesh refinement using standard diffusion (w/ extrapolated length) and the Ronen method. The reactivity difference is given by $(\Delta\rho = 1/k_{\texttt{ref}} - 1/k_{\texttt{D/RM}}) \times 10^5$, where k_D and k_{RM} are the multiplication factors of standard diffusion and the Ronen method, respectively. The reference $k_{\texttt{ref}}$ value from S_{16} is 0.744417 ($I = 400$).

A comparison of the fast and thermal fluxes, as calculated by the reference S_n code, the RM code, and a standard multigroup diffusion w/o RM correction (D_0), is shown in Fig. 4 for half-slab. The deviations (in [%]) of the RM-corrected flux and the standard diffusion (D_0) flux from the reference S_n flux is also shown in Fig. 4. The deviation from the reference solution is decreased by the Ronen iterations from approximately 20% near the boundary and 1% at the slab center to 2% and 0%, respectively.

The diffusion and transport currents calculated using the converged Ronen solution are plotted in Fig. 5. The full slab solution exhibits anti-symmetry, as expected, whereas the corrected diffusion current exhibit non-trivial behavior

Table 2. Reactivity differences as a function of mesh refinement using the Ronen method.

dx (I) [cm]	$k_{\mathtt{ref}}$	$k_{\mathtt{D}}$	$\Delta\rho_{\mathtt{D}}$ [pcm]	$k_{\mathtt{RM}}$	$\Delta\rho_{\mathtt{RM}}$ [pcm]
0.43 (50)	0.744307	0.741417	-524	0.740552	-681
0.215 (100)	0.744391	0.741355	-550	0.743447	-171
0.1075 (200)	0.744412	0.741339	-557	0.744212	-36
0.07167 (300)	0.744416	0.741336	-558	0.744356	-11
0.05375 (400)	0.744417	0.741335	-558	0.744407	-2

near the boundary. Fig. 6 show the original standard diffusion coefficients ($D = (3\sigma_{tr})^{-1}$), the RM correction terms (δD), and the corrected (spatially-dependent) diffusion D. It is clear that the diffusion correction assumes zero values at the slab center and exhibit non-trivial behavior near the boundary. The convergence of the flux (max deviation) and the criticality eigenvalue are shown in Fig. 7. While the eigenvalue converges within a few iterations, the flux exhibit slow convergence near the boundaries. The spatial flux convergence between two successive Ronen iterations is shown in Fig. 8 for the left half slab, according to $\Delta\phi = (\phi^{k-1} - \phi^k)/\phi^{k-1}$ [%]. The spatial flux convergence of the Ronen iterations with respect to the reference S_n solution for the left half slab is shown in Fig. 9.

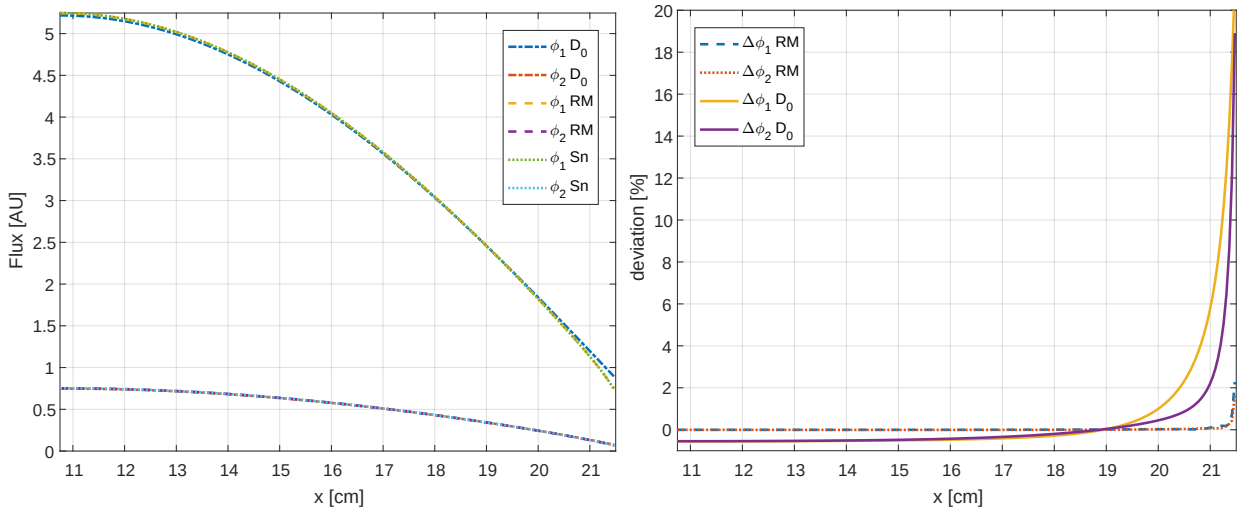

Figure 4. Comparison of the fluxes as calculated by the reference S_n code, the RM code, and a standard multigroup diffusion w/o RM correction (D_0). Results shown here after 250 Ronen iterations.

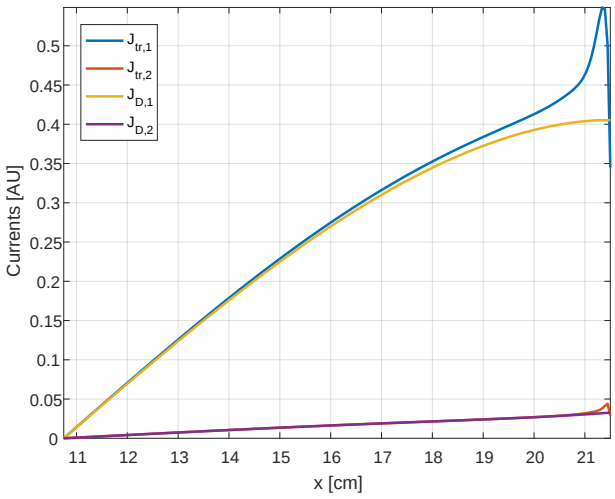

Figure 5. The diffusion and transport currents calculated using the converged Ronen solution.

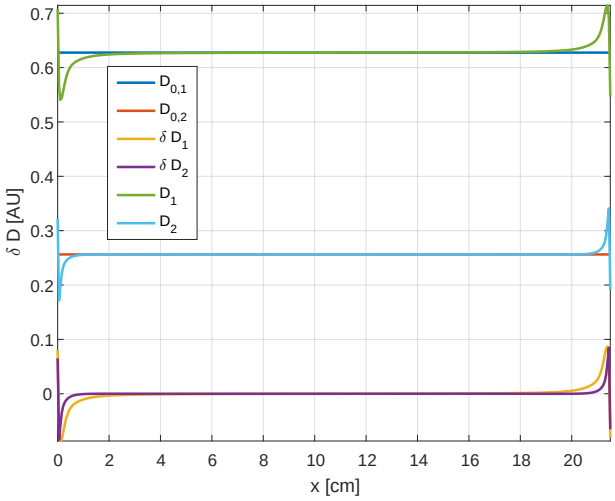

Figure 6. The original standard diffusion coefficients ($D = (3\sigma_{tr})^{-1}$), the RM correction terms (δD), and the corrected (spatially-dependent) diffusion D. Results shown here after 250 Ronen iterations.

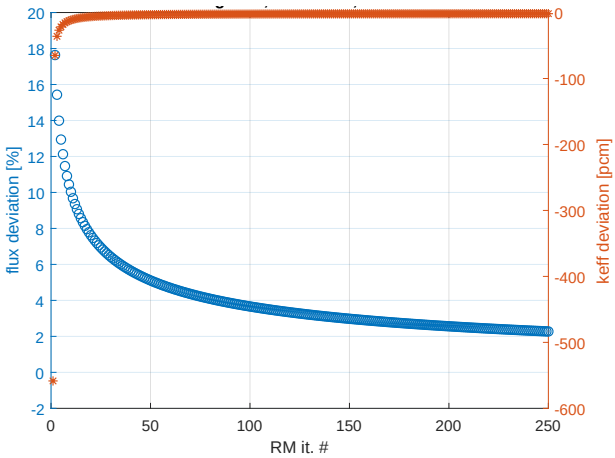

Figure 7. Convergence of the flux (max deviation) and the criticality eigenvalue.

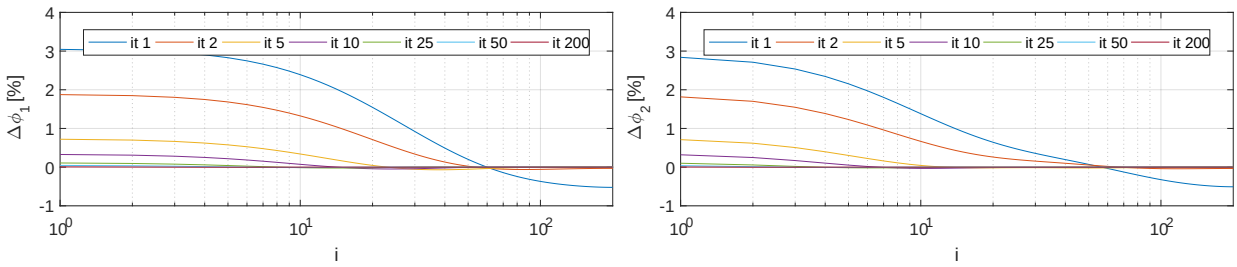

Figure 8. The spatial flux convergence between two successive Ronen iterations for the left half slab, according to $\Delta\phi = (\phi^{k-1} - \phi^k)/\phi^{k-1}$ [%].

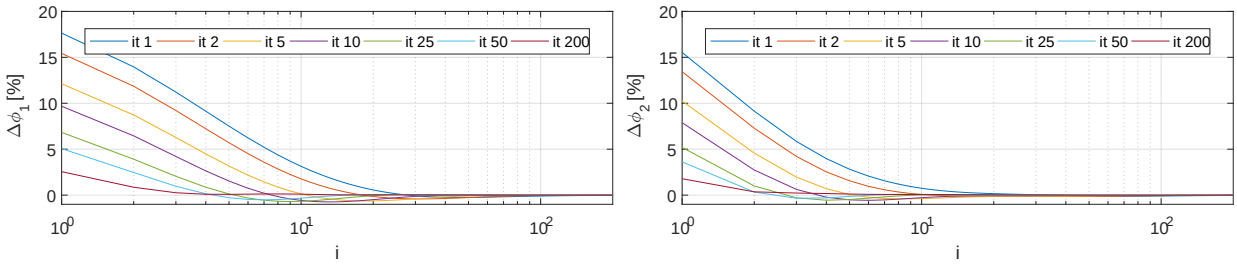

Figure 9. The spatial flux convergence of the Ronen iterations with respect to the reference S_n solution for the left half slab.

5 Conclusions

The Ronen Method was first proposed for better estimates of the diffusion coefficient by calculating the current with a higher-order transport operator and a known best-estimate neutron flux. This yielded an iterative scheme leading to new flux distributions solved by a diffusion solver but with a (spatially) modified diffusion coefficient driving the diffusion solution to that of the integral transport equation. The direct resolution of the integral equation would imply the inversion of large matrices, with poor control of their conditioning. The solution of the diffusion equation, on the other hand, offers many numerical advantages, e.g., speed and robustness. Nonetheless, the same current can be enforced in the discretized form of the diffusion equation as suggested by the CMFD, which avoids the numerical issues resulting from small flux gradients. This is the option adopted in this study.

More accurate results are obtained for the two-group benchmark problem reported in [10]. In general, slow convergence is observed for the scalar flux, whose larger discrepancy with respect to the reference is always located on the vacuum boundary. Although the method is converging to the reference results provided by a discrete ordinate transport code, the improvement of the convergence rate and the use of coarser meshes are crucial for the advancement of the methodology in practical applications. These topics will be addressed as future developments, as well as heterogeneous systems and higher-order anisotropy.

Acknowledgments

The authors express their gratitude to Prof. Yigal Ronen who initiated the idea for this study. R.G. is partially supported by the Israel Ministry of Energy, contract no. 216-11-008.

References

1. Jaeha Kim and Yonghee Kim. Development of 3-D HCMFD algorithm for efficient pin-by-pin reactor analysis. *Annals of Nuclear Energy*, 127:87–98, 2019.
2. W. R. Martin. Challenges and prospects for whole-core Monte Carlo analysis. *Nuclear Engineering and Technology*, 44(2):151–160, 2012.
3. R. D. Lawrence. Progress in nodal methods for the solution of the neutron diffusion and transport equations. *Progress in Nuclear Energy*, 17(3):271–301, 1986.
4. Kord S. Smith. Assembly homogenization techniques for light water reactor analysis. *Progress in Nuclear Energy*, 17(3):303–335, 1986.
5. F. Bertrand, N. Marie, G. Prulhière, J. Lecerf, and Seiler J. M. Comparison of the behaviour of two core designs for ASTRID in case of severe accidents. *Nuclear Engineering and Design*, 297:327–342, 2016.
6. IAEA. *Best estimate safety analysis for nuclear power plants: Uncertainty evaluation*. Number 52 in Safety Reports Series. International Atomic Energy Agency, Vienna, 2008.
7. G. I. Bell and S. Glasstone. *Nuclear reactor theory*. Van Nostrand Reinhold Company, 1970.
8. J. M. Pounders and F. Rahnema. On the diffusion coefficients for reactor physics applications. *Nuclear Sciene and Engineering*, 163:243–262, 2009.
9. P. S. Brantley and E. W. Larsen. The simplified P_3 approximation. *Nuclear Science and Engineering*, 134:1–21, 2000.
10. D. Tomatis and A. Dall'Osso. Application of a numerical transport correction in diffusion calculations. In *International Conference on Mathematics and Computational Methods Applied to Nuclear Science and Engineering (M&C 2011), Rio de Janeiro, RJ, Brazil, May 8-12, 2011*, 05 2011.
11. Y. Ronen. Accurate relations between the neutron current densities and the neutron fluxes. *Nuclear Science and Engineering*, 146(2):245–247, 2004.
12. K. S. Smith. Nodal method storage reduction by nonlinear iteration. *Transactions of the American Nuclear Society*, 44:265–266, 1983.

13. B. Davison and J. B. Sykes. *Neutron transport theory.* Oxford University Press, 1957.
14. K. M. Case and P. F. Zweifel. *Linear transport theory.* Addison-Wesley, 1967.
15. G. C. Pomraning. *The equations of radiation hydrodynamics.* Pergamon Press, Oxford, 1973.
16. J. J. Duderstadt and W. R. Martin. *Transport theory.* John Wiley & Sons, 1979.
17. E. E. Lewis and W. F. Miller. *Computational methods of neutron transport.* John Wiley and Sons, Inc.,New York, NY, 1984.
18. Milton Abramowitz and Irene A. Stegun. *Handbook of mathematical functions with formulas, graphs, and mathematical tables.* Dover Publications New York, 1964.
19. Y. A. Cengel and M. N. Özişik. Integrals involving legendre polynomials that arise in the solution of radiation transfer. *Journal of Quantitative Spectroscopy and Radiative Transfer*, 31(3):215–219, 1984.
20. J. J. Settle. Some properties of an integral that occurs in problems of radiative transfer. *Journal of Quantitative Spectroscopy and Radiative Transfer*, 52(2):195–206, 1994.
21. I. S. Gradshteyn and I. M. Ryzhik. *Table of integrals, series, and products.* Academic Press, seventh edition, 2007.